Available online at www.sciencedirect.com
SCIENCE DIRECT®
Journal of Power Sources 115 (2003) 315–322
JOURNAL OF POWER SOURCES
www.elsevier.com/locate/jpowsour

$LiMn_2O_4$-based composites processed by a chemical-route Microstructural, electrical, electrochemical, and mechanical characterization

Monica G. Lazarraga[a], Sankar Mandal[a], Joaquin Ibañez[b], J. Manuel Amarilla[a], Jose M. Rojo[a,*]

[a] *Instituto de Ciencia de Materiales de Madrid, Consejo Superior de Investigaciones Científicas, Cantoblanco, Madrid 28049, Spain*
[b] *Centro Nacional de Investigaciones Metalúrgicas, Consejo Superior de Investigaciones Científicas, Av. Gregorio del Amo 8, Madrid 28040, Spain*

Received 24 October 2002; received in revised form 12 December 2002; accepted 16 December 2002

Abstract

Composites of positive electrodes for rechargeable lithium batteries have been prepared from $LiMn_2O_4$ as electrochemically active material, carbon black (CB) as good electronic conductor, and polyvinylidenefluoride (PVDF) as binder. The composites having different contents in $LiMn_2O_4$ and CB, and nearly the same content in PVDF have been processed by a route that is currently used. The microstructure of the composites, as followed by scanning electron microscopy (SEM), is heterogeneous showing extended regions of PVDF–CB, and clusters of $LiMn_2O_4$. The electrical conductivity shows a sharp increase at the CB content of 3 vol.% (2 wt.%) in accordance with a percolation process. The capacity shows also a sharp increase at that content. A maximum in capacity at ca. 10 wt.% of CB is observed when the overall weight of the composite is taken into account. Both features, sharp increase in capacity and maximum of capacity, have been found in discharge experiments made at different currents. The composites show an elastic behavior up to a stress of ca. 6 MPa. Above this, the composites breaks down through a crack that propagates slowly according to a ductile behavior. The microstructure as well as the electrical, electrochemical, and mechanical properties of the composites are compared with those reported on composites having the same three components but processed by a different route.

Keywords: Cathode composite; Composite processing; Cathodic material; $LiMn_2O_4$; Lithium battery

1. Introduction

$LiMn_2O_4$ and $LiMn_2O_4$-based compounds all of them with spinel-type structure are electrochemically active materials for positive electrodes of rechargeable lithium batteries [1–5]. The materials are oxidized/reduced at 4–5 V depending on their transition metal ions. Thus, while voltages at ca. 4 V are associated with Mn^{3+}/Mn^{4+} oxidation/reduction [6–9], voltages at ca. 5 V are associated with the oxidation/reduction of other cations, such as Co^{3+}/Co^{4+}, Cr^{3+}/Cr^{4+}, Ni^{2+}/Ni^{4+}, etc. [10–16]. At those voltages the specific capacity, i.e. the storage charge per weight of active material, and the capacity retention on successive charge/discharge cycles (cyclability) seem to depend on the chemical composition and the synthesis chosen for preparing the active materials. Regarding the latter point, materials have been obtained through solid state reactions, Pechini method, self-combustion procedures, etc. [17–26]. Thus, while samples of nominal $LiMn_2O_4$ composition and big particle size (ca. 1 μm) have been obtained by solid state reaction [27], samples of the same composition and small particle size (ca. 30 nm) have been obtained by self-combustion procedure [28,29]. The particle size is a parameter that seems to affect the capacity, cyclability, and stability of the samples as they work as positive electrodes in rechargeable lithium cells [29–32].

The active $LiMn_2O_4$ and $LiMn_2O_4$-based materials do not work alone as positive electrodes in lithium cells. The positive electrodes are usually composites, which are made from the active material, carbon black (CB) and a polymer. Carbon black is used because its high electrical conductivity (ca. 1 S cm^{-1} at room temperature) compensates the low electrical conductivity of the active material (ca. 10^{-5} S cm^{-1} at r.t.). The polymer (PTFE, PVDF, etc.), which is an insulator, works as binder and improves handling. Despite the great

* Corresponding author. Tel.: +34-91-334-9000; fax: +34-91-372-0623.
E-mail address: jmrojo@icmm.csic.es (J.M. Rojo).

0378-7753/03/$ – see front matter © 2003 Elsevier Science B.V. All rights reserved.
doi:10.1016/S0378-7753(03)00011-9

effort done on the active materials, papers dealing with the electrode composite are still scarce [33–41]. Questions such as what is the adequate content of the three components and what is the processing that leads to composites with the best electrochemical performances are still under discussion. In a previous paper [38], some of us reported the effect of the carbon black content on the capacity of composites that were processed by cold pressing of mixtures of $LiMn_2O_4$, carbon black (CB) and polyvinylidenefluoride (PVDF). We found that the discharge capacity of the first cycle changed sharply from 0 to 135 mAh g^{-1} as a function of the relative $LiMn_2O_4$ and CB content. From the parallel study made on the electrical conductivity and the microstructure of the composites, we could establish that the discharge capacity is controlled by electron transport within the composite according to a conventional percolation process.

In this work, we have prepared composites from the three mentioned components but they have been processed by a different route. This route, hereafter so-called chemical-route, is the way the composites of positive electrodes are usually prepared. We have analyzed the discharge capacity, the electrical conductivity, the microstructure, and the strength and ductility of the composites. The results are compared with those obtained on composites processed by cold pressing of mixtures of the three components; these composites, hereafter so-called physical-route composites, are used as references.

2. Experimental

Chemical-route composites were prepared according to the following procedure: (i) polyvinylidenefluoride (PVDF) was dissolved in *N*-methyl-2-pyrrolidinone; (ii) carbon black (CB) and $LiMn_2O_4$ were added to the solution and dispersed under stirring; (iii) the solvent was evaporated by slow heating at 110 °C; and (iv) the solid was collected and cold pressed at 170 MPa to get either cylindrical pellets of 13 mm diameter or parallelepipedic pellets of 10 mm × 3 mm surface; in both cases the height was of ca. 1–2 mm. The cylindrical pellets were taken to study the electrochemical behavior and to analyze the microstructure. The parallelepipedic pellets were chosen to analyze the mechanical behavior, and both cylindrical and parallelepipedic pellets to determine the electrical conductivity. The pressure chosen for preparing the composites in this work (the chemical-route composites) was the same as for the composites previously reported (the physical-route composites) [38]. In both cases, we used the same three components. $LiMn_2O_4$ was obtained from the solid-state reaction of Mn_2O_3 and $LiNO_3$ at 750 °C according to the procedure described elsewhere [17]; the cell parameter of the cubic lattice was 8.2418(9) Å. PVDF ($M_w \approx 534000$) and CB (Super P carbon black) were commercial products supplied by Fluka and MMM Carbon, respectively. The density as determined by helium adsorption was of 1.80 g cm^{-3} for PVDF, and 1.98 g cm^{-3} for CB. The calculated crystallographic density for $LiMn_2O_4$ was of 4.28 g cm^{-3}.

Scanning electron microscopic (SEM) images were obtained in a Jeol 840 JXA microscope coupled to an energy dispersive spectrometer (EDS). Cylindrical pellets of the composites were mounted in a resin, polished in the direction along the cylinder axis, and examined by the scanning electron microscope. The direction chosen was the same as that in which the electric field was applied during the electrical and electrochemical measurements.

Two-probe electrical measurements were carried out in a 1260 Solartron impedance/gain phase analyzer. The frequency range chosen was 5–10^6 Hz. Four-probe electrical measurements were done in-line configuration; a dc current (1–100 mA) was applied through the two external electrodes and the voltage drop was measured between the two internal electrodes. In the two kind of measurements, the electrodes were obtained from a silver paint. All measurements were carried out at room temperature.

Electrochemical measurements were carried out in a lithium cell in which the negative electrode was a lithium-metal foil, the electrolyte was 1 M $LiPF_6$ solution in anhydrous ethylene carbonate and dimethyl carbonate (1:1 weight ratio), and the positive electrode was the composite. The two electrodes and the electrolyte were assembled in a Swagelock-type cell within an argon glove box in which the water content was below 1 ppm. The cells were galvanostatically cycled in an Arbin instrument (model BT 2043) between 3.3 and 4.5 V at constant currents of *C*/24, *C*/12, and *C*/5. *C* is the capacity of the cathode calculated from the theoretical capacity of $LiMn_2O_4$ (148 mAh) and the mass of this compound in the composite. The values 24, 12, and 5 are the discharge times expressed in hours.

Mechanical measurements were done by the three points bending technique on parallelepiped samples of 10 mm length, 3 mm width, and 1.8 mm depth (Fig. 1). The span

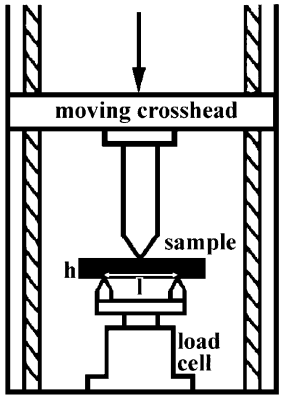

Fig. 1. Three points bending technique used to determine the stress and strain of the composite pellets. The parallelepiped pellet is placed between two supports; *h* and *l* stand for the height of the pellet and the length between supports, respectively. The cross-head is moving down at a constant speed.

length, i.e. the distance between the two supports, was of 7 mm. The cross-head speed was of 0.005 mm s^{-1}. Two test were done on the chemical-route composite and physical-route one, both having the same composition: 8.5 wt.% CB, 81.5 wt.% $LiMn_2O_4$, 10 wt.% PVDF.

3. Results and discussion

3.1. Composites

The chemical-route composites prepared according to the procedure described in the Section 2 are outlined in Table 1. In this table besides the weight and volume of the three components (PVDF, $LiMn_2O_4$, and CB), we have included the volume of air we estimated for each composite pellet. The volume of the three components was calculated from their mass and density. The volume of air was estimated from subtraction of the total volume of the pellet to the volume occupied by the three components. In Fig. 2, we show how changes the volume content of $LiMn_2O_4$, Air and PVDF as a function of the volume content of CB. This plot shows that: (i) the PVDF content decreases slightly along the series; (ii) the $LiMn_2O_4$ content decreases clearly as the CB content increases because the former is gradually replaced by the latter; and (iii) the air content increases as the CB content increases. Although these trends are similar to those found for the physical-route composites [38], we should note that the chemical-route composites show higher air contents than the physical-route ones; thus, for the chemical-route composite and physical-route composite both having 20 vol.% CB, the air content is 50 vol.% in the former and 30 vol.% in the latter. In accordance with it, the $LiMn_2O_4$ content is lower in the chemical-route composite (20 vol.% $LiMn_2O_4$) than in the physical-route one (35 vol.% $LiMn_2O_4$). Composites with air contents (porosity) below 5 vol.% have been obtained through a process that is based on a hot-extrusion of powder mixtures of the components [37]. For our chemical- and physical-routes composites, the PVDF content is close (10–15 vol.%) along the two series.

Table 1
Weight (wt) and volume (v) contents of PVDF, $LiMn_2O_4$, CB, and air for the composites prepared by the chemical-route

Composite	PVDF		$LiMn_2O_4$		CB		Air
	wt (%)	v (%)	wt (%)	v (%)	wt (%)	v (%)	v (%)
CR-0	9.3	15.6	90.7	64.2	0	0	20.2
CR-1.4	9.5	13.3	89.4	53	1.1	1.4	32.8
CR-2	9.4	15.5	89.3	62	1.4	2	20.5
CR-2.5	9.5	13.4	88.5	52	2	2.5	32.1
CR-3.2	9.4	14.9	88.5	58.9	2.2	3.2	23
CR-3.4	9.4	15.2	88.3	60	2.3	3.4	21.4
CR-4.7	9.2	14.5	87.5	57.9	3.3	4.7	22.9
CR-5.6	10	12.8	85.2	45.8	4.8	5.6	35.9
CR-6.5	10	12.1	84	42.9	6	6.5	38.6
CR-8.3	10	10.9	81.5	36.7	8.5	8.3	44
CR-8.6	10	12.7	82.7	44.4	7.3	8.6	34.3
CR-11.2	11	12.4	78	36.9	11	11.2	39.4
CR-14.5	11	10.4	72	28.4	17	14.5	46.7
CR-18.7	11	9.1	64	22.2	25	18.7	50
CR-23.6	13	8.9	49	13.8	38	23.6	53.7

The composites are labeled as CR followed by the CB volume content.

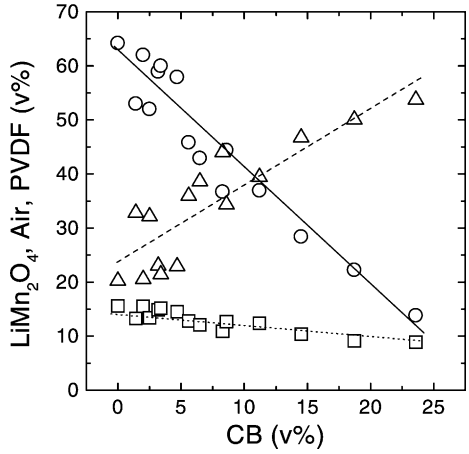

Fig. 2. Variation of the volume content of $LiMn_2O_4$ (circles), air (triangles), and PVDF (squares) as a function of the CB volume content. The lines are drawn to guide the eye.

3.2. Electrical conductivity

The total conductivity (dc conductivity) of the chemical-route composites as a function of the CB volume content is shown in Fig. 3. The conductivity changes from ca. 10^{-5} to ca. 1 S cm^{-1}, which correspond to the conductivity of $LiMn_2O_4$ alone [11,42–44] and CB alone [35,38,45,46], respectively. Since $LiMn_2O_4$ is an n-type semiconductor [42,44] and CB shows a metal behavior [37,45,46], the conductivity of the composites is of electronic type. The contributions of PVDF and air to the composite conductivity

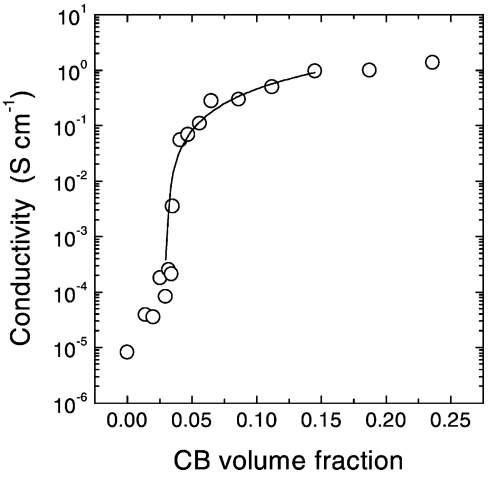

Fig. 3. Electrical conductivity vs. carbon black volume fraction. The solid line is the best fitting to the equation $\sigma = \sigma_0(v - v_c)^t$; the fitting parameters are $\sigma_0 = 18$ S cm^{-1}, $v_c = 0.03$, $t = 1.4$.

are negligible because they are insulators. The conductivity increases sharply for CB volume fractions close to 0.03. The experimental data are well fitted to an equation of the form $\sigma = \sigma_0(v - v_c)^t$, for $v \geq v_c$, that accounts for a percolation process [47]. In this equation v is the CB volume fraction, v_c is the CB volume fraction at the percolation threshold, t the exponent, and σ_0 is a pre-exponential factor. From this fitting, we deduce $v_c = 0.03$, i.e. 3% by volume of CB. Percolation thresholds of 2–6 vol.% have been reported for other CB-based composites [35,37]. Below the percolation threshold, the conductivity of our composites is dominated by the conductivity of $LiMn_2O_4$; above that, the conductivity is mainly due to the contribution of CB. The percolation threshold found is the same as for the physical-route composites [38] but the exponent and pre-exponential factor are different from those of the physical-route composites. It suggests us some differences in the microstructure of the two kinds of composites that could be more important as the CB content increases.

3.3. Microstructure

The SEM images obtained on the chemical-route CR-5.6 composite are shown in Fig. 4a and 4b. For comparison, the SEM image obtained on a physical-route (6.4 vol.% CB, 52.4 vol.% $LiMn_2O_4$, 14.7 vol.% PVDF, 26.5 vol.% Air) composite is shown in Fig. 4c. Both composites have similar CB contents (5.6 and 6.4 vol.%), and in both cases the CB content is close to the percolation threshold (3 vol.%). In the chemical-route composite (Fig. 4a), we can distinguish white and black regions. From the microanalysis done we could detect Mn in the white regions, and F and C in the black ones. So, we ascribe the white regions to $LiMn_2O_4$, and the black regions to CB and PVDF. The size of the white regions (1–10 μm), much bigger than the size of individual particles of $LiMn_2O_4$ (0.1–1 μm) [38], indicates that they are clusters of $LiMn_2O_4$ particles. The black regions seem to be interconnected giving rise to a network along the composite; this network, which was not observed in the physical-route composites, is a feature of the chemical-route composites. The different values of C and F found in the network suggest us a variation in the relative content of PVDF and CB; the network seems to be PVDF impregnated with CB. The size of the black regions, much bigger than the individual particles of PVDF (1–10 μm) [38], points to a growth of the PVDF particles associated with the processing of the composite. Since PVDF is first dissolved in *N*-methyl-2-pyrrolidinone and then the solvent is evaporated, the individual PVDF particles can coalesce into bigger particles. A magnification of the square marked region of Fig. 4a is shown in Fig. 4b. We can see that the extended shape of the black regions is clearly different from the starting granular shape of PVDF. However, the granular shape of PVDF is maintained in the physical-route composite as shown in Fig. 4c; in this image some of the PVDF particles are marked by arrows. In the chemical-route composite besides

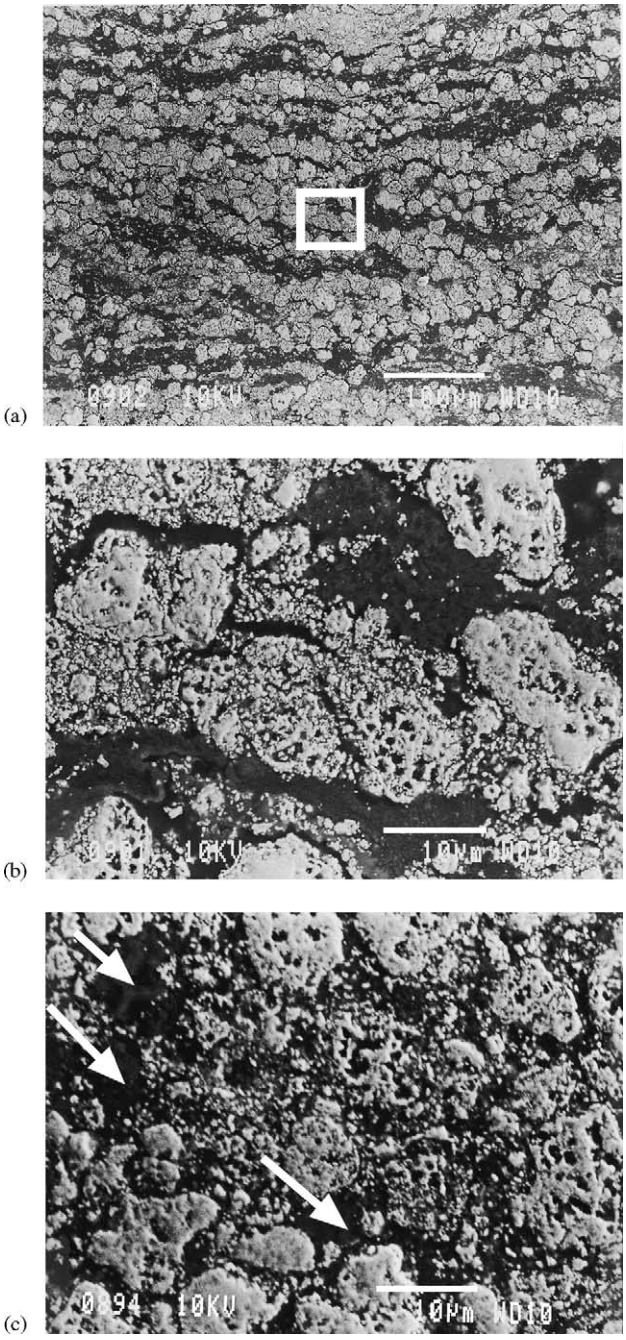

Fig. 4. SEM micrographs obtained on the chemical-route CR-5.6 composite (a and b) and on a physical-route composite (c). The image (b) is a magnification of the square marked region in image (a). The composition of the physical-route composite is: 6.4 vol.% CB, 52.4 vol.% $LiMn_2O_4$, 14.7 vol.% PVDF, 26.5 vol.% Air.

the extended black regions already mentioned, we can see small black spots within the white regions (Fig. 4b). Since PVDF has the trend to give extended black regions, the small black spots would be ascribed to CB and/or air but we could not distinguish between them.

The SEM images of the chemical-route CR-18.7 composite and the physical-route (32.2 vol.% CB, 19.2 vol.% $LiMn_2O_4$, 13 vol.% PVDF, 36.5 vol.% Air) composite, both

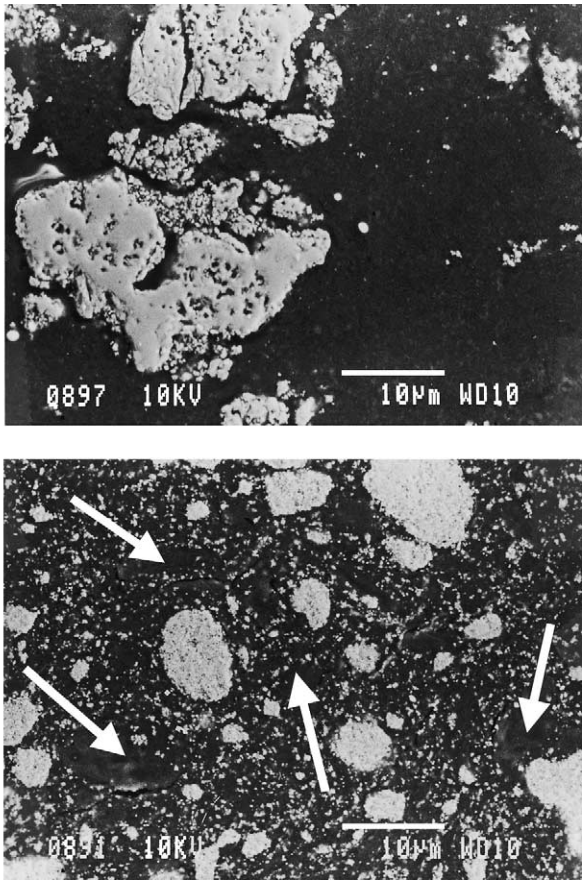

Fig. 5. SEM micrographs obtained on the chemical-route CR-18.7 composite (a) and on a physical-route composite (b). The composition of the physical-route composite is: 32.2 vol.% CB, 19.2 vol.% $LiMn_2O_4$, 13 vol.% PVDF, 36.5 vol.% Air.

having a CB content much higher than that at the percolation threshold, are shown in Fig. 5. In the chemical-route composite (Fig. 5a), we can see that $LiMn_2O_4$ is more heterogeneously distributed than in the physical-route one (Fig. 5b). Indeed, the white clusters are bigger in the former, and in this composite we do not observe the small white clusters found in the latter. The black regions show an extended shape in the chemical-route composite (Fig. 5a) as already mentioned. In the physical-route composite (Fig. 5b), some granular black particles (arrows marked) can be distinguished; these particles are ascribed to PVDF. The components CB and air are considered to be included in the black regions of the two images.

3.4. Electrochemical behavior

The discharge curves (not shown) obtained at the *C*/24, *C*/12, and *C*/5 current are similar to the curves reported elsewhere [1–9]. These curves show at ca. 4 V a two-step plateau from which the capacity can be estimated. The capacity of the first discharge corresponding to the chemical-route composites is plotted as a function of the CB volume fraction in Fig. 6. For the three mentioned currents, we observe a

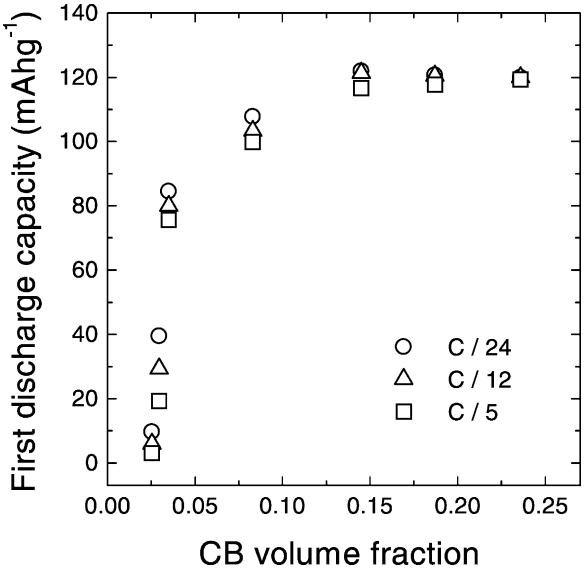

Fig. 6. First discharge capacity vs. CB volume fraction. Circles, triangles, and squares stand for the experiments made at the *C*/24, *C*/12, and *C*/5 current, respectively. The discharge capacity is referred to the weight of the active material ($LiMn_2O_4$).

sharp increase in capacity at CB volume fractions close to 0.03. Above this value, the capacity increases gradually and attains a plateau. The shape of the capacity curve and the sharp increase found at the CB volume fraction of 0.03, which coincides with the percolation threshold deduced from the conductivity curve, point out that the capacity also follows a percolation process. Since the electrical conductivity curve accounts for the electron transport within the composite, and the discharge capacity curve accounts for the insertion of Li^+/e^- into the active material, both electron transport and insertion process are clearly associated. Electron transport within the composite up to the active material allows Mn^{4+}/Mn^{3+} reduction and Li^+ insertion.

In accordance with the mentioned percolation model, at least one conducting path due to aggregation of CB particles (presumably the PVDF–CB regions) should be established at the percolation threshold [47]. The presence of the conducting path accounts for the sharp increase in capacity observed. For CB contents above the percolation threshold, the gradual increase in capacity up to ca. 120 mAh g^{-1} can be interpreted as an increase in the number of conducting paths. The amount of the active material that is accessible to the Li^+/e^- insertion must increase as the number of conducting paths increases. In Fig. 6, we can see that for high CB volume fractions (0.23) the capacity measured at the three mentioned currents is nearly the same. However, as the CB content decreases from that value to the percolation threshold (0.03), systematic differences in capacity for the three currents are found; thus, the capacity measured at *C*/5 (high current) is lower than the capacity measured at *C*/12, and this capacity is lower than that measured at *C*/24 (low current). Since the decrease in capacity as the current increases is usually associated with kinetic restrictions of

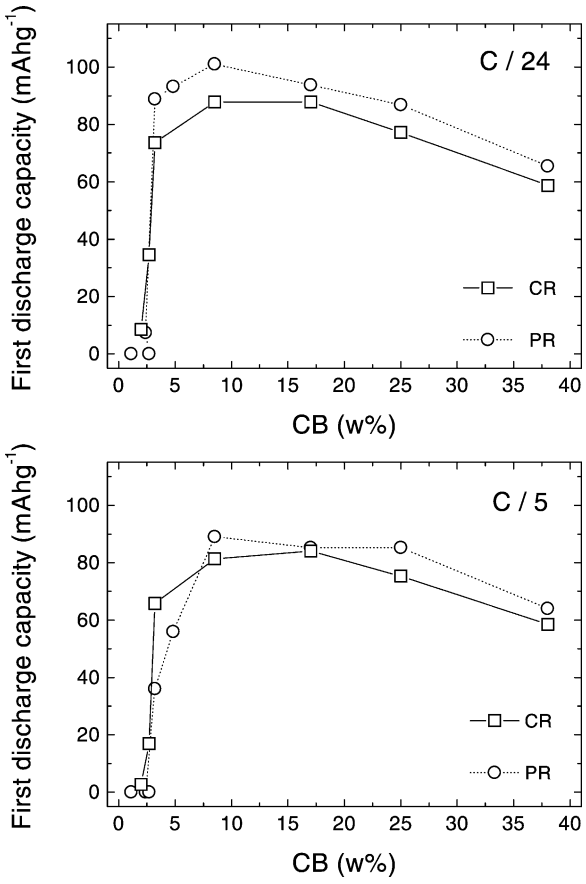

Fig. 7. First discharge capacity vs. CB weight content. The discharge capacity is referred to the overall weight of the composite electrode. The experiments were made at the *C*/24 and the *C*/5 current. In both cases, the squares stand for the chemical-route composites. For comparison, the data obtained at those currents on physical-route composites (circles) are included.

Li^+/e^- insertion into the active material, the kinetic is much more important in composites whose CB content is close to the percolation threshold (few conducting paths) than in composites having higher CB contents (more conducting paths).

A comparison of the discharge capacity found for the chemical-route and physical-route composites is shown in Fig. 7. In this figure, we have plotted the data obtained at two currents: *C*/24 (low current) and *C*/5 (high current). In the ordinate axis, the discharge capacity is referred to the overall weight of the electrode, i.e. to the weight that includes the active material, CB and PVDF. The CB content in the abscissa axis is now referred to the weight instead of the volume. For both currents, the discharge capacity increases sharply at the percolation threshold (2.5 wt.% or 3 vol.% of CB) and at higher weights the capacity goes through a maximum whose position is close to 10 wt.% CB. The presence of the maximum indicates that it is possible to optimize the composition of the composite; the broad shape of the maximum, however, indicates that the optimization can be got in a range of CB weights. At the left of the maximum the increase in capacity as the CB weight increases can be explained in terms of an increase in the number of conducting paths; Li^+/e^- insertion into the active material occurs more efficiently because more active material is accessible. At the right of the maximum the capacity decreases because, despite the continuous increase in the number of conducting paths, the amount of active material decreases; indeed, $LiMn_2O_4$ is progressively replaced by CB as the latter component increases (Fig. 2). In Fig. 7, we also see that above the percolation threshold, the capacity of the physical-route composites (circles) is slightly higher than that of the chemical-route ones (squares). The lower capacity found for the latter composites would be associated with: (i) a part of the active material remains embedded in insulating PVDF regions; and (ii) the active material is more agglomerated in the chemical-route composite as already mentioned.

3.5. Mechanical characterization

The measurements were done on chemical- and physical-route composites having a composition (8.5 wt.% CB, 81.5 wt.% $LiMn_2O_4$, 10 wt.% PVDF) whose CB content corresponds to the maximum in capacity of Fig. 7. We have chosen the three points bending test (Fig. 1) because it is especially useful for brittle materials [48] and shows clear differences between the chemical-route and physical-route composite. The stress (σ) and strain (ε) are calculated according to the expressions [49]:

$$\sigma = \frac{3Fl}{2wh^2}$$

and

$$\varepsilon = \frac{6h\delta}{l^2}$$

where F is the load; l, w and h are the span length, width and height of the sample; δ is the deflection increment at the midspan. Two tests were done on each composite the data being reproducible.

The stress-strain curve for the chemical-route composite (dotted line) and for the physical-route composite (solid line) are shown in Fig. 8. In the elastic regime, i.e. where σ versus ε shows a linear dependence ($\varepsilon < 0.02$), the slope is close in both cases indicating similar elastic modulus: 277 and 235 MPa for the physical-route and chemical-route composite, respectively. In that figure, σ attains a maximum value of 5.5 MPa for the physical-route composite and of 6.5 MPa for the chemical-route composite; it indicates that the strength is higher for the chemical-route composite. On increasing ε ($\varepsilon > 0.02$ for the physical-route composite and $\varepsilon > 0.03$ for the chemical-route one) a decrease of σ is observed in the two cases, but the decrease is clearly different. While σ decreases sharply for the physical-route composite, that decreases gradually for the chemical-route composite; these behaviors agree with a rapid propagation of

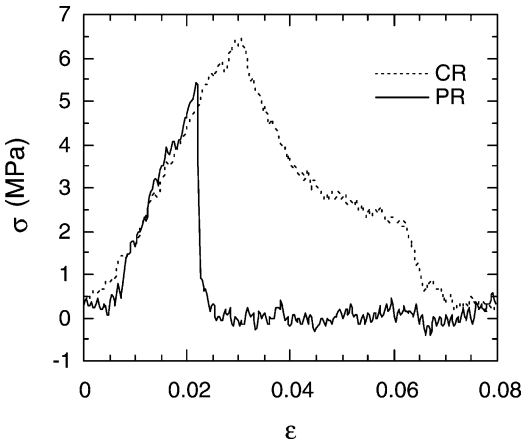

Fig. 8. Stress (σ) vs. strain (ε) for the chemical-route composite (dashed line) having the composition 8.5 wt.% CB, 81.5 wt.% $LiMn_2O_4$, and 10 wt.% PVDF. For comparison, the σ–ε curve recorded on a physical-route composite (solid line) having the same composition as the chemical-route composite is shown.

the crack in the former case and a slow propagation in the latter one. The PVDF–CB network of the chemical-route composite can account for the ductile behavior found; the lack of that network is accompanied by a fragile behavior of the physical-route composites.

4. Concluding remarks

Positive electrodes for rechargeable lithium batteries having different $LiMn_2O_4$/CB ratios have been prepared as composites by an usual procedure here called the chemical-route. These composites have been compared with analogous composites prepared from mixtures of the components (the physical-route).

Although the two types of composites are rather similar about their electrical conductivity, they show differences in microstructure, discharge capacity and mechanical behavior. The microstructure of the chemical-route composites shows extended PVDF–CB regions, contrary to the physical-route composites in which individual particles of PVDF remains isolated each other. The discharge capacity of the chemical-route composites is slightly lower than that of the physical-route composites. The chemical-route composites are ductile, and hence they are more easily handled than the physical-route composites.

Acknowledgements

Financial support by the Spanish Ministry of Science and Technology through the project MAT 2001-0562 is gratefully acknowledged. One of the authors (M.G.L.) thanks the Spanish Ministry of Education, Culture and Sports for a fellowship.

References

[1] M.M. Thackeray, P.J. Johnson, L.A. de Picciotto, P.G. Bruce, J.B. Goodenough, Mater. Res. Bull. 19 (1984) 179.
[2] M. Wakihara, O. Yamamoto, Lithium Ion Batteries: Fundamentals and Performance, Wiley, Tokyo, 1998.
[3] C. Julien, Z. Stoynov, Materials for Lithium-Ion Batteries, Nato Sciences Series. Kluwer Academic Publishers, Dordrecht, 1999.
[4] M.M. Thackeray, J. Am. Ceram. Soc. 82 (1999) 3347.
[5] N. Terada, T. Yanagi, S. Arai, M. Yoshikawa, K. Ohta, N. Nakajima, A. Yanai, N. Arai, J. Power Sources 100 (2001) 80.
[6] D. Guyomard, J.M. Tarascon, Solid State Ionics 69 (1994) 222.
[7] G. Li, H. Ikuta, T. Uchida, M. Wakihara, J. Electrochem. Soc. 143 (1) (1996) 178.
[8] P. Arora, B.N. Popov, R.E. White, J. Electrochem. Soc. 145 (3) (1998) 807.
[9] J.M. Amarilla, J.L. Martín de Vidales, R.M. Rojas, Solid State Ionics 127 (2000) 73.
[10] Q. Zhong, A. Bonakdarpour, M. Zhang, Y. Gao, J.R. Dahn, J. Electrochem. Soc. 144 (1) (1997) 205.
[11] H. Kawai, M. Nagata, H. Kageyama, H. Tukamoto, A.R. West, Electrochim. Acta 45 (1999) 315.
[12] L. Hernan, J. Morales, L. Sanchez, J. Santos, Solid State Ionics 118 (1999) 179.
[13] H. Shigemura, H. Sakaebe, H. Kageyama, H. Kobayashi, A.R. West, R. Kanno, S. Morimoto, S. Nasu, M. Tabuchi, J. Electrochem. Soc. 148 (7) (2001) A730.
[14] C. Sigala, A. Le Gal La Salle, Y. Piffard, D. Guyomard, J. Electrochem. Soc. 148 (8) (2001) A812.
[15] E. Zhecheva, R. Stoyanova, M. Gorova, P. Lavela, J.L. Tirado, Solid State Ionics 140 (2001) 19.
[16] S. Mandal, R.M. Rojas, J.M. Amarilla, P. Calle, N.V. Kosova, V.F. Anufrienko, J.M. Rojo, Chem. Mater. 14 (2002) 1598.
[17] J.M. Amarilla, Bol. Soc. Ceram. Vidrio 34 (1995) 463.
[18] Y. Gao, J.R. Dahn, J. Electrochem. Soc. 143 (1) (1996) 100.
[19] C. Tsang, A. Manthiram, Solid State Ionics 89 (1996) 305.
[20] X. Qiu, X. Sun, W. Shen, N. Chen, Solid State Ionics 93 (1997) 335.
[21] V. Massarotti, D. Capsoni, M. Bini, G. Chiodelli, C.B. Azzoni, M.C. Mozzati, A. Paleari, J. Solid State Chem. 147 (1999) 509.
[22] T. Le Mercier, J. Gaubicher, E. Bermejo, Y. Chabre, M. Quarton, J. Mater. Chem. 9 (1999) 567.
[23] E.N. Zhecheva, M.Y. Gorova, R.K. Stoyanova, J. Mater. Chem. 9 (1999) 1559.
[24] M. Mohan Rao, C. Liebenow, M. Jayalakshmi, H. Wulff, U. Guth, F. Scholz, J. Solid State Electrochem. 5 (2001) 348.
[25] Z.P. Guo, S. Zhong, G.X. Wang, G. Walter, H.K. Liu, S.X. Dou, J. Electrochem. Soc. 149 (2002) A792.
[26] K.M. Shaju, G.V. Subba Rao, B.V.R. Chowdari, Solid State Ionics 148 (2002) 343.
[27] T. Nakamura, A. Kajiyama, Solid State Ionics 124 (1999) 45.
[28] K.-M. Lee, H.-J. Choi, J.-G. Lee, J. Mater. Sci. Lett. 20 (2001) 1309.
[29] D. Kovacheva, H. Gadjov, K. Petrov, S. Mandal, M.G. Lazarraga, L. Pascual, J.M. Amarilla, R.M. Rojas, P. Herrero, J.M. Rojo, J. Mater. Chem. 12 (2002) 1184.
[30] G.G. Amatucci, C.N. Schmutz, A. Blyr, C. Sigala, A.S. Gozdz, D. Larcher, J.M. Tarascon, J. Power Sources 69 (1997) 11.
[31] D. Aurbach, M.D. Levi, K. Gamulski, B. Markovsky, G. Salitra, E. Levi, U. Heider, L. Heider, R. Oesten, J. Power Sources 81–82 (1999) 472.
[32] D. Ahn, M. Song, J. Electrochem. Soc. 147 (3) (2000) 874.
[33] A. Momchilov, V. Manev, A. Nassalevska, J. Power Sources 41 (1993) 305.
[34] D.H. Jang, S.M. Oh, Electrochim. Acta 43 (1998) 1023.
[35] N. Probst, E. Grivei, H. Smet, J.B. Soupart, ITE Battery Lett. 1 (1999) 64.

[36] A. Momchilov, A. Trifonova, B. Banov, B. Pourecheva, A. Kozawa, J. Power Sources 81–82 (1999) 566.
[37] G.B. Appetecchi, M. Carewska, F. Alessandrini, P.P. Prosini, S. Passerini, J. Electrochem. Soc. 147 (2) (2000) 451.
[38] S. Mandal, J.M. Amarilla, J. Ibáñez, J.M. Rojo, J. Electrochem. Soc. 148 (1) (2001) A812.
[39] L. Fransson, T. Eriksson, K. Edstrom, T. Gustafsson, J.O. Thomas, J. Power Sources 101 (2001) 1.
[40] J.K. Hong, J.H. Lee, S.M. Oh, J. Power Sources 111 (2002) 90.
[41] N.-S. Choi, Y.-G. Lee, J.-K. Park, J. Power Sources 112 (2002) 61.
[42] V. Massarotti, D. Casponi, M. Bini, G. Chiodelli, C.B. Azzoni, M.C. Mozzati, A. Paleari, J. Solid State Chem. 131 (1997) 94.
[43] E. Iguchi, N. Nakamura, A. Aoki, Philos. Mag. B 78 (1998) 65.
[44] J. Molenda, K. Swierczek, W. Kucza, J. Marzec, A. Stoklosa, Solid State Ionics 123 (1999) 155.
[45] M. Hindermann-Bischoff, F. Ehrburger-Dolle, Carbon 39 (2001) 375.
[46] F. El-Tantawy, K. Kamada, H. Ohnabe, Mater. Lett. 57 (2002) 242.
[47] D. Stauffer, A. Aharony, Introduction to the Percolation Theory, Taylor & Francis, London, 1994.
[48] M.F. Ashby, D.R.H. Jones, Engineering Materials, Pergamon Press, Oxford, 1986.
[49] American Society for Testing and Materials 1990, Standard test methods for bend testing of metallic flat materials for spring applications involving static loading, ASTM designation E855-90, Philadelphia, 1990.